A major purpose of the Technical Information Center is to provide the broadest dissemination possible of information contained in DOE's Research and Development Reports to business, industry, the academic community, and federal, state and local governments.

Although a small portion of this report is not reproducible, it is being made available to expedite the availability of information on the research discussed herein.

1

LA-UR -87-352

CONF-8608163--1

Los Alamos National Laboratory is operated by the University of California for the United States Department of Energy under contract W-7405-ENG-36

LA-UR--87-352

DE87 006068

TITLE PATTERN SELECTION AND COMPETITION IN NEAR-INTEGRABLE SYSTEMS

AUTHOR(S) A. R. Bishop
D. W. McLaughlin

SUBMITTED TO The Proceedings of Conference "Structure, Coherence and Chaos in Dynamical Systems," Lyngby, Denmark, August 1986, by "Manchester University Press (1987".

DISCLAIMER

Los Alamos Los Alamos National Laboratory
Los Alamos, New Mexico 87545

FORM NO 836 R4
ST NO 2629 5/81

Pattern Selection and Competition in Near-Integrable Systems

by

A. R. Bishop
Theoretical Division and
Center for Nonlinear Studies
Los Alamos National Laboratory
Los Alamos, NM 87545

and

D. W. McLaughlin
Program in Applied Mathematics
University of Arizona
Tucson, AZ 85721

Abstract

Pattern selection and competition in certain near-integrable systems is discussed. These systems provide models for controlled studies of low dimensional attractors in high (infinite) dimensional systems. Four examples from damped, driven pendulum rings are summarized in the order of increasing spatial complexity of their chaotic attractors. These examples illustrate the use of numerical and analytical techniques from soliton mathematics to study properties of chaotic attractors. In particular, the connection of (unperturbed) homoclinic states with instabilities of spatial patterns, with interactions between patterns, and as possible sources of temporal chaos is emphasized.

I. Introduction

Complex systems often exhibit rich spatial and temporal patterns, which possess both coherent and chaotic features. This property is found in many physical systems (water waves, plasmas, turbulent fluids, laser light, solid state and electronic devices), as well as in numerical simulations of partial differential equations and cellular automata.[1] Analysis of such complicated systems is extremely limited; thus, usually one is restricted to numerical or physical observations.

Although these complex systems have high (even infinite) dimensional phase spaces, their chaotic attractors are often low dimensional. (At least this low dimensionality seems to apply to the macroscopic transport via collective structures.) Recently theorists, using methods from the mathematical theory of dynamical systems, have made considerable progress in discovering and understanding universal properties of low dimensional systems. These theoretical developments have given considerable insight toward the interpretation of observations of the long time behavior of complex systems. However, a mathematical theory of chaotic attractors for infinite dimensional systems is still in its infancy.

Our own recent research has focused on model partial differential equations which are far simpler than realistic physical systems, yet complicated enough to possess low dimensional attractors in an infinite dimensional state space. Typically we study one dimensional nonlinear wave equations which are nearby "integrable" equations. These model problems permit a detailed (at times even analytical) study of specific properties of chaotic attractors in a high dimensional system. In particular, we use these models to develop intuition about the nature of

the chaotic attractors and the mechanisms which cause pattern selection, competition between patterns, and the generation of chaos. Some of these features, which can be understood in detail for the model problems, are rather general and will extend to more realistic systems where such detailed investigations are impossible at present -- nor can they be anticipated in the near future.

In this article, we will briefly describe several representative examples, in order of the increasing spatial complexity of their attractors, which illustrate the above philosophy. The reader should consult the references for further details. All of the examples which we discuss here are perturbed sine-Gordon equations, which provide elegant model problems.

II. Homogeneously AC Driven, Damped Pendulum Ring

A concrete example is the damped, ac-driven sine-Gordon equation under periodic boundary conditions:

$$\phi_{tt} - \phi_{xx} + \sin\phi = \varepsilon[-\alpha\phi_t + \Gamma \sin(\omega t)] \quad , \tag{2.1}$$

$$\phi(x + L, t) = \phi(x,t) \quad , \tag{2.1bc}$$

$$\phi(x, t = 0) = \phi_{in}(x) \quad , \tag{2.1ic}$$

$$\phi_t(x, t = 0) = v_{in}(x) \quad .$$

Here $0 < \varepsilon \ll 1$, and the control parameters are α (the strength of the dissipation), Γ (the amplitude of the ac driver), ω (the frequency of the ac driver), L (the spatial period), and the initial data (ϕ_{in}, v_{in}). This equation models a chain of harmonically coupled nonlinear pendula,

with periodic boundary conditions describing a ring configuration. Note that both the dissipation and driving are spatially homogeneous. Historically this system with no spatial structure (i.e., the single pendulum) has provided a useful model to direct and test one's understanding of temporal chaos in deterministic dynamical systems.[2,3] However, these studies of the single pendulum neglect all effects of spatial structure which, when present, can completely alter the nature of the space-time attractor.

In numerical experiments[4,5] with weak homogeneous perturbations and single humped initial data, the fundamental phenomenon is a resonance between a spatially localized excitation (a "breather") and the ac driver. (It should be mentioned that the driving frequency ω is chosen less than unity in order to resonate with a spatially localized breather whose natural frequency ω_{Br} satisfies $0 < \omega_{Br} < 1$. If one drives at an $\omega > 1$, one resonates with extended phonons whose natural frequencies satisfy $1 < \omega_{ph} < \infty$.) Above a low threshold driving strength Γ, the initialized excitation adjusts, persists, and locks periodically to the driver. As the system is further stressed by increasing Γ, this locked state looses stability and more complicated spatial structures emerge. As parameter values are varied, the attractors can be temporally periodic, quasi-periodic, subharmonically locked, or chaotic (with intermittancy). Depending principally on the frequency ω of the ac driver, the chaotic dynamics is controlled by either (i) "breather $\leftrightarrow$ kink-antikink" or (ii) "breather $\leftrightarrow$ radiation" transitions. These distinct types of nonlinear modes (kinks, breathers, and anharmonic radiation) classify regimes of chaotic evolution.

The reader will notice that the terms "kink," "breather," and "anharmonic radiation" have not been defined. In general such definitions are not precise, involving approximate techniques such as collective coordinate methods. It is especially difficult to distinguish between breathers and radiation. A major advantage in working near an integrable soliton equation is that nonlinear spectral transforms exist which provide a precise definition and classification of these distinct nonlinear modes. A detailed description of the application of nonlinear spectral methods to chaotic attractors of system (2.1) may be found in Refs. (6,7). These nonlinear spectral methods have allowed us to demonstrate that a chaotic attractor can be comprised of a small number of nonlinear modes which undergo collision, annihilation, nucleation, decay, and transition between coherent and extended states. In addition these spectral methods have identified the presence of infinite period homoclinic orbits which are associated with transitions between the three types of nonlinear modes. We believe that these homoclinic states, although less familiar than the pendulum separatrix, play as fundamental a role in this chaotic pendulum chain. On the one hand, these homoclinic states are related to instabilities which generate more complicated spatial patterns; on the other hand, the infinite period states act as sources of extreme sensitivity which can produce chaos. A main result of the nonlinear spectral method is to establish numerically the presence of frequent homoclinic crossings along the chaotic attractor.

We describe two cases. First, we fix the driving frequency ω less than, and not near, unity.[4,5,6] For example, at $\omega = 0.6$ and $\varepsilon\alpha = 0.2$,

Then the bifurcation sequence as a function of increasing stress parameter Γ is given symbolically by

$$\begin{pmatrix} \text{Flat} \\ \text{Periodic} \end{pmatrix} \rightarrow \begin{pmatrix} \text{1 Excitation} \\ \text{Periodic} \end{pmatrix} \rightarrow \begin{pmatrix} \text{2 Excitations} \\ \text{Periodic} \end{pmatrix} \rightarrow \begin{pmatrix} \text{2-4 Excitations} \\ \text{Chaotic} \end{pmatrix}$$

$$\rightarrow \begin{pmatrix} \text{4 Excitations} \\ \text{Periodic} \end{pmatrix} \rightarrow \ldots$$

In these symbols the top entry of each ordered pair describes the spatial structure of the attractor, while the second entry indicates its temporal behavior.

Such bifurcation sequences may be understood as follows: As a function of increasing stress, the flat attractor becomes unstable to a $k_1 (= 2\pi/L)$ Fourier excitation which saturates into an attractor with one localized breather per spatial period. With further stress, this single breather develops a $k_2 (= 4\pi/L)$ instability which may saturate into two breathers per period or one breather plus a k_2 anharmonic phonon, depending principally on dissipation strength. (The first situation of period halving into two breathers occurs at larger dissipation.) When the attractor contains a k_2 anharmonic phonon, the temporal behavior may be quasi-periodic, subharmonically locked, or chaotic depending upon parameter values. Similar distinctions apply as the system is further stressed and four spatial excitations emerge (arising from a $k_4 (= 8\pi/L)$ instability).

In this low frequency ($\omega \simeq 0.6$) case, the chaotic regimes are characterized by "breather" to "kink-antikink" transitions since the breathers which resonate with a low frequency ac driven have large amplitude ($\sim 2\pi$) and thus are near the kink-antikink threshold.

Figure 1 shows how, in the chaotic regime, the basic coherent structures persist, but that their phase-locking relative to each other has been (chaotically) broken so that the structure fails to repeat by a small amount after each driver period. We can decompose the field at each instant of time into radiation and either two "breathers" or two "kinks" and two "antikinks". Furthermore, chaotic evolution of $\langle\phi(t)\rangle$ (the spatial average of ϕ) through multiples of 2π does not take place via single particle dynamics but rather through the slow diffusion of the kinks (antikinks). Our nonlinear spectral analysis indeed confirms the presence of a small number of localized excitations in the chaotic attractor.[6] This small number of dominating localized modes suggests that the chaos may be governed by a low dimensional strange attractor. We have checked that the correlation dimension[6,8] is indeed low (~3). In fact, the chaos observed in this experiment is intermittent between the periodic locked states [Figure (1a) and its period-4 analogue] and the irregularly evolving unlocked states [Figure (1b)]. This intermittency is reflected in the time series for the spatial averages of u and u_t, shown in Figure 2.

We close our discussion of this experiment by emphasizing that, at these low driving frequencies, breather to kink-antikink breakup dominates the chaotic attractor. A homoclinic state in the unperturbed system is associated with this transition. This infinite period state admits a familiar physical interpretation and provides a natural source of sensitivity. In the next experiment, we describe a nonlinear Schrödinger (NLS) regime which is dominated by the breather to radiation transition, whose homoclinic states are far less familiar,[9,10] but similarly important as potential sources of NLS chaos.

Next, we consider the second case with a higher driving frequency ω near, but still less than, unity.[7,11] For example, consider $\omega = 0.87$ and $\varepsilon\alpha = 0.04$. (One difficulty with the experiments at smaller ω (e.g., $\omega \simeq .6$) is that the interesting bifurcations occur at rather large values of the stress parameter ($\varepsilon\Gamma \simeq 1.0$). These perturbations are large enough that analysis based on the integrable sine-Gordon theory is not appropriate. When ω is raised to $\omega \simeq .9$, the interesting bifurcations occur at much small values of the stress parameter making analysis based on the integrable theory more appropriate. The choice $0 \ll \omega \tilde{<} 1$ places us in the "nonlinear Schrödinger (NLS) regime". That is, when $\omega \tilde{<} 1$, one can use perturbation methods to approximate a class of equations, (which includes the sine-Gordon equation (2.1)) by an NLS equation:

$$u(x,t) = \sqrt{6\varepsilon}[A(\varepsilon t, \sqrt{\varepsilon}x)e^{it} + c.c.] \quad .$$

Here the complex amplitude $A(T,X)$ satisfies

$$-2iA_T + A_X + 3AA^*A = i\alpha A + \Gamma^{\varepsilon}e^{-i(1-\omega)T} \quad ,$$

where $\Gamma^{\varepsilon} = \Gamma/2\sqrt{6\varepsilon}$. Thus, because of the generic nature of NLS, this particular experiment at $\omega \lesssim 1$ actually applies to a wide class of physical problems.[12-18]

At these parameter values ($\omega = 0.87$, $\varepsilon\alpha = .04$) numerical experiments on the initial value problem (2.1) reveal a beautiful route to chaos with the following features:

(i) temporally - one frequency → two frequencies → chaos;

(ii) spatially - one localized "hump" → two localized "humps";

(iii) symmetry changes and pattern competition;

(iv) low dimensional, yet chaotic, attractors;

(v) temporal intermittency, accompanied by spatial symmetry changes.

All of this action occurs at small values of the bifurcation parameter ($\varepsilon\Gamma \lesssim 0.12$); hence, even the chaotic system is, in some sense, near-integrable. As the stress parameter $\varepsilon\Gamma$ increases, the attractor changes according to the following symbolic sequence:

$$\begin{pmatrix}\text{Flat}\\ \text{Periodic}\end{pmatrix} \rightarrow \begin{pmatrix}1\ \text{Excitation}\\ \text{Periodic}\end{pmatrix} \rightarrow \begin{pmatrix}2\ \text{Excitations}\\ \text{Quasi-Periodic}\end{pmatrix}$$
$$\rightarrow \begin{pmatrix}1\ \text{Excitation}\\ \text{Periodic}\end{pmatrix} \rightarrow \begin{pmatrix}2\ \text{Excitations}\\ \text{Quasi-Periodic}\end{pmatrix} \rightarrow \begin{pmatrix}2\ \text{Excitations}\\ \text{Chaotic}\end{pmatrix}.$$

We briefly comment on these attractors. Their space-time behavior is depicted in Figure 3. For small driving amplitudes ($0.0 < \varepsilon\Gamma < 0.058$), the periodic spatial structure of the initial conditions decays as a transient, and the attractor is an x-independent flat state with no spatial structure. This state is periodic in time with the period of the ac driver. As this flat state is further stressed (by increasing $\varepsilon\Gamma$), it loses stability and the new attractor which emerges has the spatial structure of one breather-like hump per spatial period riding over a flat background. Its temporal behavior remains periodic at the driving frequency. As $\varepsilon\Gamma$ is still further increased, this state of one hump per period loses its stability to a new attractor which has two humps per spatial period (one being localized in space and the second with the character of $k = 2$, extended, anharmonic radiation), and two temporal frequencies (one at the driving frequency $\omega = 0.87$, and the

second at much lower frequency). Temporally, the state can be either quasi-periodic or subharmonically locked to the driver. With further increase of $\varepsilon\Gamma$, the attractor returns to the (1Ex,P) state, and then back to (2Ex,QP) (with, again, one localized and one extended hump). We have not measured the structure of such "windows" in detail. As $\varepsilon\Gamma$ increases further, the two humps per period "dance" irregularly, rather than quasi-periodically, and both are localized.

With the stress parameter $\varepsilon\Gamma$ fixed well within the chaotic region, the spatial structure of this chaotic attractor contains two humps per period, just as the milder (2Ex,QP) attractor. The difference between these two spatial structures is as follows: In the quasi-periodic case (2Ex,QP), one of the humps is rather extended; in the chaotic case (2Ex,C), both humps are localized and the state is almost spatially period halved. These two localized humps dance, decay into radiation, reform through radiation, focus and grow back into localized states, develop relative center of mass motion, collide, and generally interact chaotically.

Finally, we describe the attractor at $\varepsilon\Gamma$ values just above the chaotic threshold. Here the attractor is temporally intermittent. The time series for the energy $\langle H\rangle = \int dx[\frac{1}{2}\phi_t^2 + \frac{1}{2}\phi_x^2 + 1-\cos\phi]$ and the average displacement $\langle\phi\rangle = \int dx\phi$ are depicted in Figure 3 for $\varepsilon\Gamma = .1055$. Note the long, linearly growing "laminar" regions separated by chaotic bursts. In these laminar regions the attractor is the same as the quasi-periodic attractor at slightly lower values of $\varepsilon\Gamma$. It has two humps per period, one localized and the second $k = 2$ anharmonic radiation. Temporally, it acts quasiperiodically. As the $k = 2$ radiation grows and focuses into a more localized hump, the amplitude of the time

series (Figure 4) grows linearly; finally the time series "bursts". In this region of time, the attractor at $\varepsilon\Gamma = .1055$ is very similar to the chaotic attractor at higher $\varepsilon\Gamma$ values which was described in the preceding paragraph. It contains two localized humps which dance, decay, and interact chaotically. As $\varepsilon\Gamma$ is increased from .1055, the percentage of time the attractor resides in the quasi-periodic "laminar" regions decreases, as is to be expected for intermittency.

We have claimed that the temporal bifurcation sequence is $P \rightarrow QP \rightarrow C$. In order to deduce this, we tested the numerical data with standard diagnostics of dynamical systems theory (phase planes, Poincare sections, temporal power spectra, leading Lyapunov exponent, and correlational dimension). These tests are described in detail elsewhere.[7,11] Here we restrict ourselves to the phase planes of Figure 5, and the power spectra of Figure 6.

We note: (i) All diagnostics are consistent with the above scenario. (ii) The correlation dimension changes with increasing $\varepsilon\Gamma$ as $1. \rightarrow 2. \rightarrow 3.5 \rightarrow 4.3$. The dimension of 3.5 occurs at $\varepsilon\Gamma = .1055$, where the attractor is intermittent, and it can be interpreted as a "weighted average" of 2 and 4.3. The rise from $2 \rightarrow 3.5$ occurs rapidly, between $\varepsilon\Gamma = .105$ and $\varepsilon\Gamma = .0155$. (iii) The power spectra plots, Figure 6, show that the laminar region of the intermittent attractor indeed acts as if it were quasi-periodic in time.

Nonlinear spectral measurements[7,11] show that only a few ($\sim$3 or 4) nonlinear modes are appreciably excited - even when the attractor is chaotic. The number of appreciably excited modes increases with $\varepsilon\Gamma$, changing when the attractor changes to within the accuracy of our study:

(F,P): 1 Mode - k_0

(1Ex,P): 2 Modes - k_0; b_1

(2Ex,QP): 3 Modes - k_0, k_2, b_1

(2Ex,C): 3-4 Modes -

In this list, k_0 stands for flat, x independent radiation, k_2 represents anharmonic extended radiation similar to $\cos(2\cdot\frac{2\pi}{L}x)$, and b_1 denotes one localized "breather" per period. In the case of the chaotic attractor we do not list the type of nonlinear modes because those which are present change with time; at some times (k_0, k_2, b_1, b_1) are present, while at other times (k_0, k_1, k_2, b_1), etc. (Actually, even in the quasiperiodic attractor, the excitation changes between a localized breather b_1 and extended anharmonic k_1 radiation.) Thus, at a fixed value of the stress $\varepsilon\Gamma$, the chaotic attractor consists in a few nonlinear modes which change their type as a function of time. These type changes constitute interactions and transitions between radiation and localized spatial states.

Homoclinic orbits and homoclinic crossings: The spatially periodic, integrable sine-Gordon equation[9,10] has homoclinic orbits separating radiation modes from localized modes. In this NLS regime, the most important homoclinic state is that which separates the breather from an anharmonic k_1 phonon.[10,11] We have used the nonlinear spectral transform to check directly the presence of these homoclinic crossings along this chaotic attractor. As the system is sufficiently stressed to access either large amplitude quasi-periodic or chaotic attractors, these numerical measurements detect frequent homoclinic crossings of k_1 - b_1 type, which were just discussed.

Thus, homoclinic crossings of $k_1 \leftrightarrow b_1$ type are present, and these are potential sources of chaos in the NLS regime. While the measurement of such $k_1 \leftrightarrow b_1$ states is straight forward with nonlinear spectral projections, it is quite inaccessible by standard data analysis such as spatial and temporal profiles, time series diagnostics, or linear spectral transforms.

III. DC Driven, Damped Pendulum Ring

One might imagine that a homogeneously dc driven, damped ring of pendula would exhibit little spatial structure. However, this perturbation actually yields a very rich variety of space-time patterns which illustrate a number of important general phenomena including transverse instabilities on moving interfaces and spatial competition among nonlinear modes.

The model problem is as in equation (2.1), except that we replace "$\Gamma \sin \omega t$" with a dc driver "Γ_{dc}". Again, the most interesting regime is one of small dissipation ($\varepsilon\alpha \lesssim 1$) where there is a distinctive hysteresis. Namely as $\varepsilon\Gamma_{dc}$ is increased from 0, there is no mean rotation ($\langle\phi_t\rangle$) until $\varepsilon\Gamma_{dc} = 1$, where the pendula begin to rotate homogeneously in space and with an oscillatory time dependence about $\langle\phi_t\rangle$. As $\varepsilon\Gamma_{dc}$ is now decreased, a finite value of $\langle\phi_t\rangle$ persists for $\varepsilon\Gamma_{dc} < 1$, accompanied by the spontaneous appearance of time dependent spatial patterns. The hysteresis diagram is organized into "steps" (see Figure 7.), each of which is associated with specific spatial structures. These may be locked breather wave trains (anharmonic standing waves) or tranversly moving kink-antikink pairs.

Linear stability analysis of the x-independent rotating state can be used to predict the periodicity of the emerging structures on the high steps very satisfactorily.[19] These structures saturate in the nonlinear sine-Gordon potential into breather wave trains, in that their amplitudes and widths have breather characteristics. These nonlinear structures compete for transverse space. This competition is resolved in two distinct ways: (1) amplitude delocking of the breather wavetrain producing breathers of different sizes (see Figure 8); or (2) breather break-up into kink-antikink pairs. The latter occurs on the lower steps where the "washboard frequency is smaller; and hence, the resonant breathers have large amplitudes and thus easily break into kink-antikink pairs.

Clearly there are a large variety of sources of low dimensional chaos in this situation. Mathematically, homoclinic crossings, such as those discussed in section 2, are certainly present. Physically chaos may be induced either through irregular jumping between steps or through transitions between patterns on the same step.

IV. Inhomogeneously AC Driven, Damped Pendulum Ring

In the previous sections we found: (i) that an ac driver could introduce a characteristic length scale -- the width of the saturated (breather) modes which resonate temporally with the driver; and (ii) that competition between spatial patterns results when this length scale is inconsistent with the total length available per hump. In this section we consider an experiment[20] which tunes this competition by controlling two length scales. This control is achieved with a spatially periodic ac driving term of the form $\Gamma \sin(\omega t - qx)$. Again, the

frequency ω controls the width of the saturated mode. However, now the driver introduces an additional spatial scale, $2\pi/q$. In effect, this driver resonates with the localized breathers of frequency ω and with phonons of wave number q. If the two length scales are near commensurate, a strong temporally periodic locking of a breather wave train of spatial periodicity $2\pi/q$ occurs, even for very high driving strengths (See Figure 9a). However, if the two length scales are incommensurate, even very small driving strengths produce complex space-time patterns (see Figure 9b). In this manner we can begin to study the temporal evolution of complicated (chaotic?) spatial patterns.

V. Conclusions

In this article we have described several examples of coherence and chaos in near integrable systems. Such models are simple enough to allow careful, controlled studies of low dimensional chaos in a high dimensional setting. In particular, the spatial patterns of the attractor are closely related to solutions of the nearby integrable system, and a nonlinear spectral transform can be used to quantify properties of these spatial structures. In some instances such measurements show that the attractor can be represented by a small number of nonlinear modes; however, these modes must continally change their type between radiation and localized states as the phase point evolves along the attractor. Thus, these nonlinear spectral measurements establish the importance of soliton-radiation interactions on the chaotic attractor. In addition, these measurements detect frequent homoclinic crossings as the phase point evolves along the attractor. The homoclinic states are related to instabilities which generate more

complicated spatial patterns, and they act as sources of sensitivity which can produce temporal chaos. A main result of the nonlinear spectral measurements of these chaotic attractors is to establish numerically the presence of frequent homoclinic crossings.

Of course, systems near soliton equations must have special properties. Nevertheless, the discovery and verification of the behavior of their chaotic attractors is much easier than in general situations. Consider, as an example, the detailed information which we described in this article about homoclinic crossings in the perturbed sine-Gordon equation. Given the importance of homoclinic crossings in the near integrable situation, we can now begin to ask about the possibility of homoclinic states separating distinct spatial patterns in more general settings.

For the future, it remains to be seen which of the chaotic phenomena identified in near soliton systems will persist in a more general framework. In the near integrable framework, we are continuing to develop an analytical reduced description of attractors that incorporates the relevant small subset of interacting nonlinear modes, as well as the dynamical features of homoclinic orbits.

References

1. See articles in Spatio-Temporal Coherence and Chaos in Physical Systems, Proceedings of Los Alamos Workshop, edited by A. R. Bishop, G. Grüner, and B. Nicolaenko, Physica 23D (1986).

2. D. D'Humieres, M. Beasley, B. Huberman, and A. Libchaber, Phys. Rev. A 26, 3483 (1982); J. Crutchfield, J. Farmer, and B. Huberman, Phys. Reports 92, 42 (1983).

3. J. Guckenheimer and P. Holmes, Nonlinear Oscillations, Dynamical Systems, and Bifurcations (Springer, New York, 1983).

4. A. R. Bishop, K. Fesser, P. S. Lomdahl, W. C. Kerr, M. B. Williams, and S. E. Trullinger, Phys. Rev. Lett. 50, 1095 (1983).

5. A. R. Bishop, K. Fesser, P. S. Lomdahl, and S. E. Trullinger, Physica 7D, 259 (1983).

6. E. A. Overman, D. W. McLaughlin, and A. R. Bishop, Physica 19D, 1 (1986).

7. A. R. Bishop, M. G. Forest, D. W. McLaughlin, and E. A. Overman, Physica 23D, 293 (1986).

8. P. Grassberger and I. Procaccia, Phys. Rev. Lett. 50, 346 (1983).

9. N. Ercolani, M. G. Forest, and D. W. McLaughlin, Physica 18D, 472 (1986).

10. N. Ercolani, M. G. Forest, and D. W. McLaughlin, "Homoclinic Orbits for the Periodic Sine-Gordon Equation," in preparation (1986).

11. A. R. Bishop, D. W. McLaughlin, and E. A. Overman, "A Quasi-Periodic Route to Chaos in a Near Integrable PDE: Homoclinic Crossings," Univ. of Arizona preprint (1986).

12. G. D. Doolen, D. F. DuBois, and H. Rose, Phys. Rev. Lett. 51, 335 (1983).

13. H. T. Moon, P. Huerre, and L. G. Redekopp, Physica 7D, 135 (1983).

14. D. W. McLaughlin, J. V. Moloney, and A. C. Newell, Phys. Rev. Lett. 51, 75 (1983).

15. J. Wu, R. Keolian, and I. Rudnick, Phys. Rev. Lett. 52, 1421 (1984).

16. H. T. Moon and M. V. Goldman, Phys. Rev. Lett. 53, 1921 (1984).

Figure Captions

Fig. 1 Space-time evolutions of $\phi(x,t)$ for the SG system through two driving periods for $\varepsilon\alpha = 0.2$, $\omega = 0.6$, with periodic boundary conditions, and driving strengths (a) $\varepsilon\Gamma = 0.8$, which results in periodic time evolution; (b) $\varepsilon\Gamma = 1.0$, which results in chaotic kink-antikink motions (nearly repeating every driving period).

Fig. 2 Spatial average $\langle\phi\rangle(t)$ and phase-plane for the chaotic regime at $\varepsilon\Gamma = 1.0$ (Fig. 1b), showing intermittency: laminar regimes are time-periodic and spatially locked 2-breather (Fig. 1a).

Fig. 3. Space-time profiles on the attractor: (a) $\varepsilon\Gamma = 0.050$ (flat in space, periodic in time); (b) $\varepsilon\Gamma = 0.105$ (quasi-periodic); (c) $\varepsilon\Gamma = 0.110$ (chaotic). Note the second hump centered at $x = \pm 12$ in the quasi-periodic case. Note also the changes in spatial symmetry in the chaotic case.

Fig. 4. The energy, H, and mean value of the waveform, $\langle\phi\rangle$, as a function of time for $\varepsilon\Gamma = .1055$ (chaotic). Note the long growing laminar region for $11,300 < t < 13,200$ and the chaotic regions which bound it.

Fig. 5. Phase planes for $\varepsilon\Gamma =$ (a) 0.101 (periodic); (b) 0.102 (quasi-periodic); (c) 0.104 (quasi-periodic); (d) 0.105 (quasi-periodic), and (e) 0.1055 (chaotic).

Fig. 6. a) The power spectra at selected values of $\varepsilon\Gamma$.

b) Temporal power spectra for selected time intervals in the chaotic regime.

Fig. 7. A summary of numerical results. The arrows indicate the direction in which the driving, Γ_{dc}, was adiabatically changed. The x's on the periodic steps (labeled P-N) denote where the periodic symmetry breaks to another P-N state (see Fig. 8) when Γ_{dc} is increased, and the o's indicate where the symmetry is regained as Γ_{dc} is decreased. Notice that for $0.15 \leq \Gamma_{dc} \leq 0.18$ on the 3K-3K step, the spatial pattern is periodic. The nomenclature reflects an annular Josephson junction context for definiteness. (See Pagano et al, those proceedings, for the effect of the ϕ_{xxt} dissipation.)

Fig. 8. Two examples of coexisting attractors on the same step: (a) periodic 6 (P-6) standing breather train whose lengths compete with higher driving, yielding the amplitude delocking illustrated; (b) the P-4 state may undergo kink-antikink breakup to give the $4K + 4\bar{K}$ state shown, whose kinks and antikinks move transversely. On each of the ϕ axes, ϕ is given modulo 2π.

Fig. 9. Snapshots of ϕ and ϕ_t, and power spectra, for spatially-dependent driving $\Gamma \sin(\omega t - kx)$, of a sine-Gordon ring with $L = 24$, $\varepsilon\alpha = 0.1$ and $\omega = 0.9$: (a) $2\pi/k = 6$, $\varepsilon\Gamma = 1.1$ and (b) $2\pi/k = 24$, $\varepsilon\Gamma = 0.5$. In case (a), the resonant breather length scale is $\approx 2\pi/k$ and locked, time-periodic response occurs even with large driving strengths. In case (b), the two length scales are very different and a low-dimensional chaotic, spatially-irregular attractor is found even at small driving strengths.

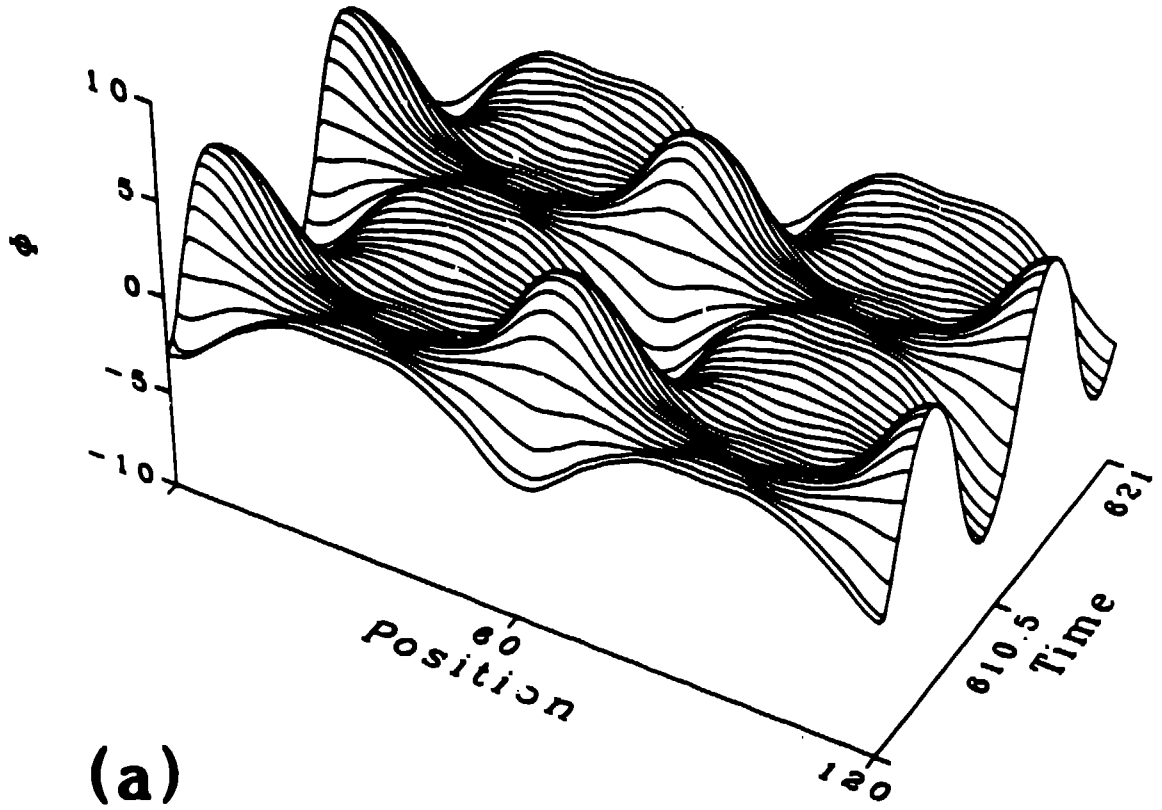
10
5
0
-5
-10
φ
60
Position
120
610.5
Time
621

(a)

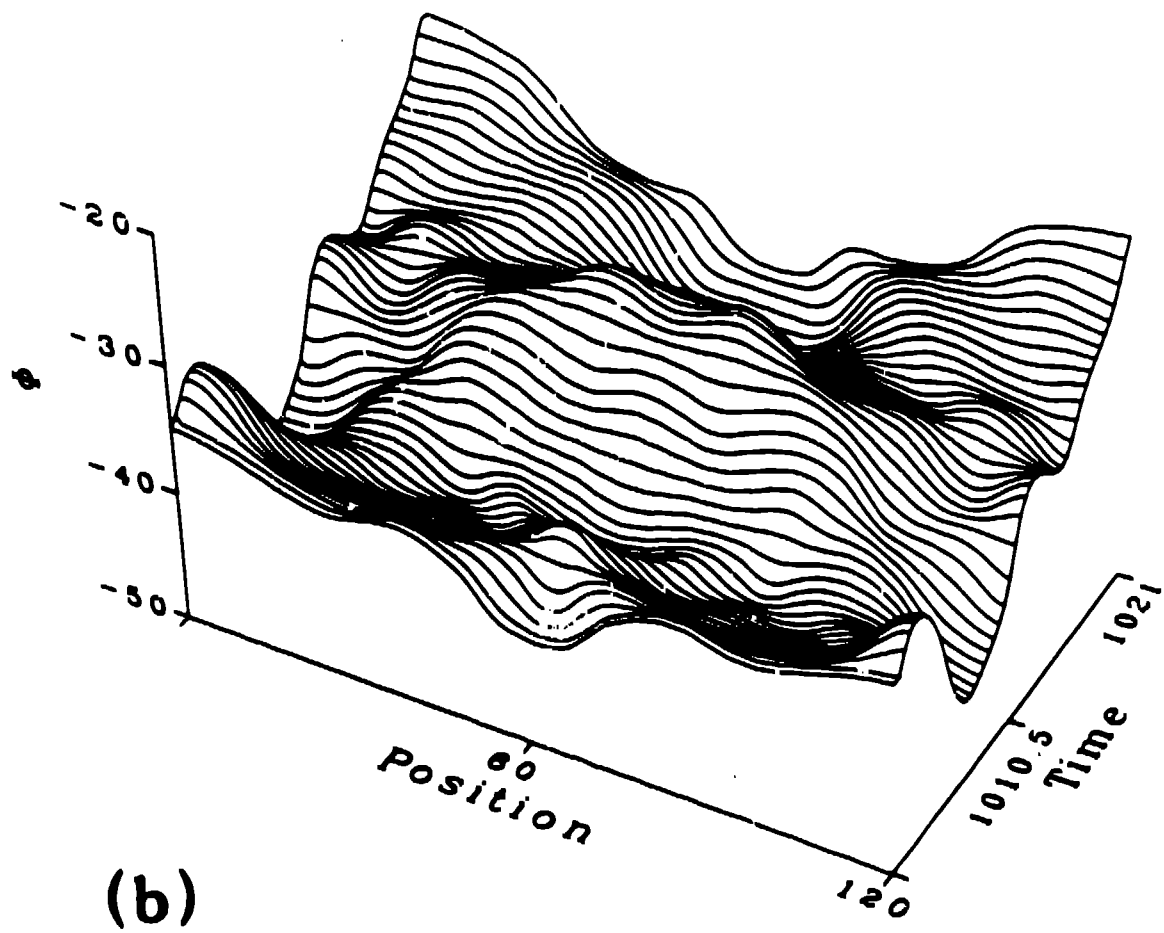
-20
-30
-40
-50
φ
60
Position
120
1010.5
Time
1021

(b)

FIG.1.

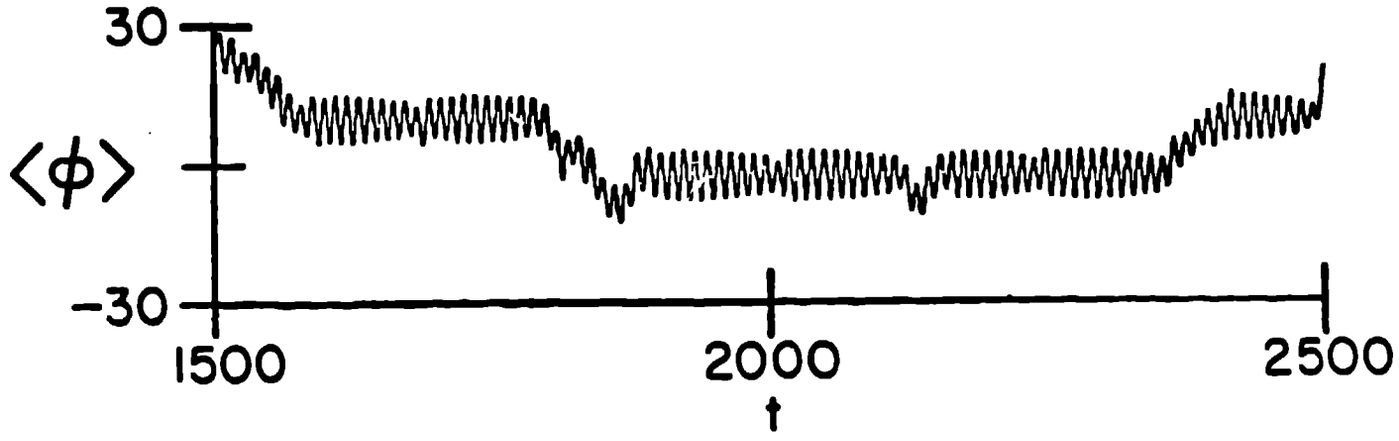

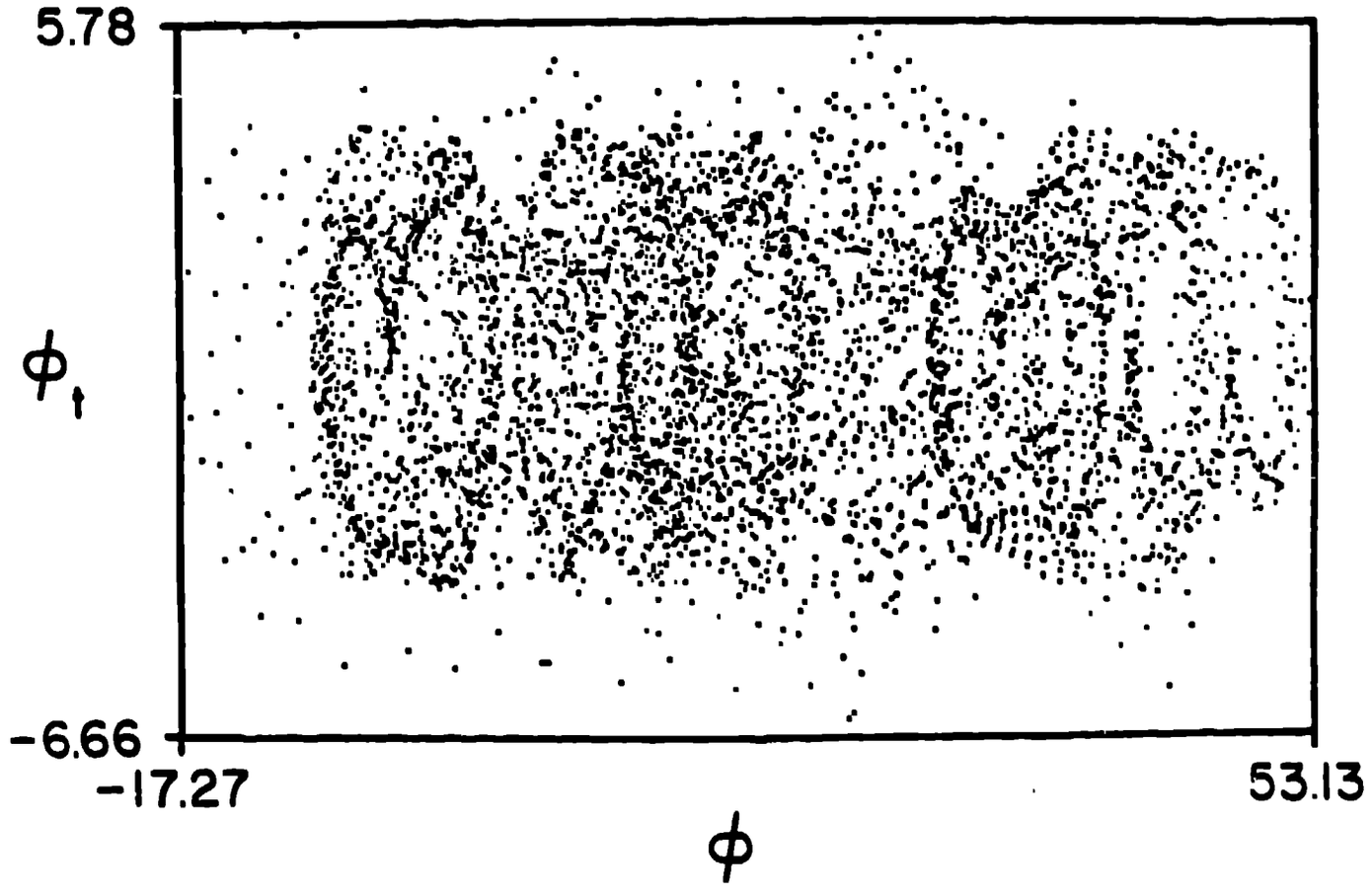

FIG. 2.

a)

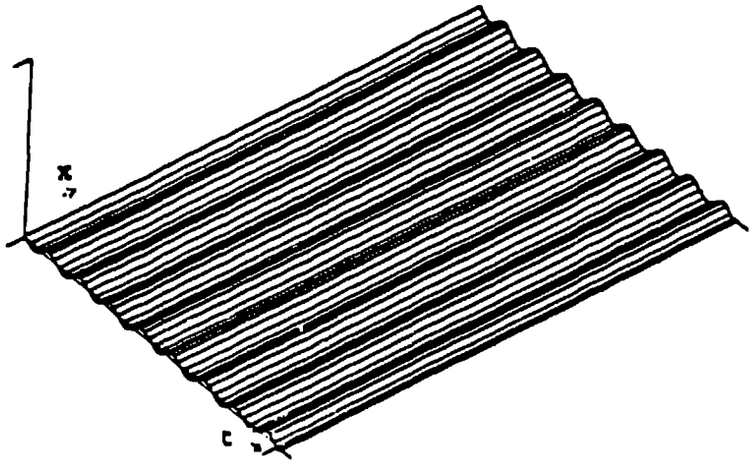

b)

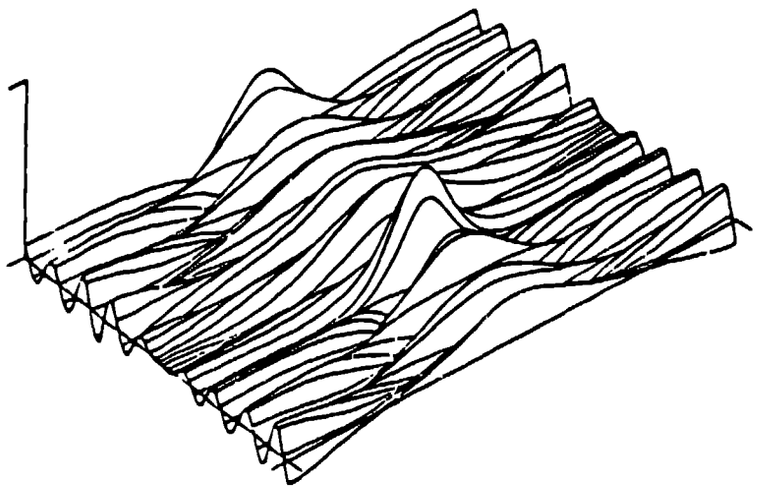

c)

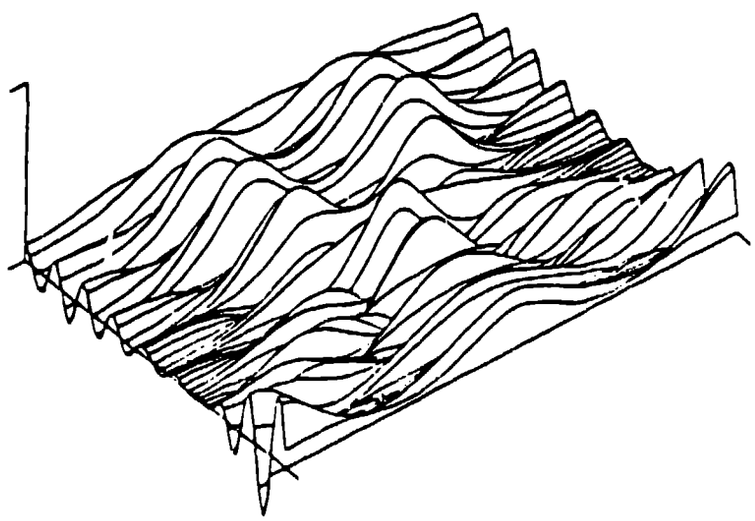

FIG. 3

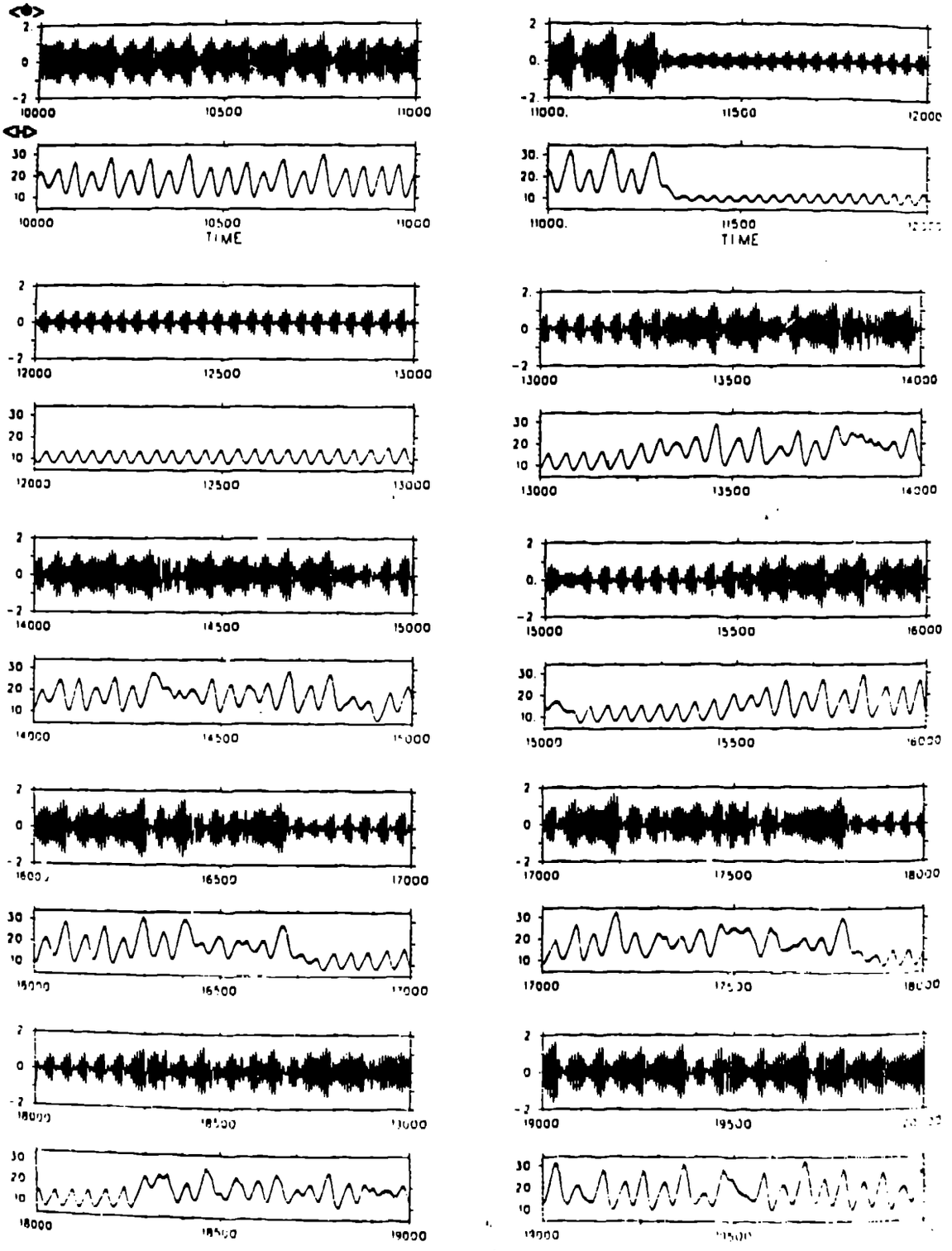

FIG. 4.

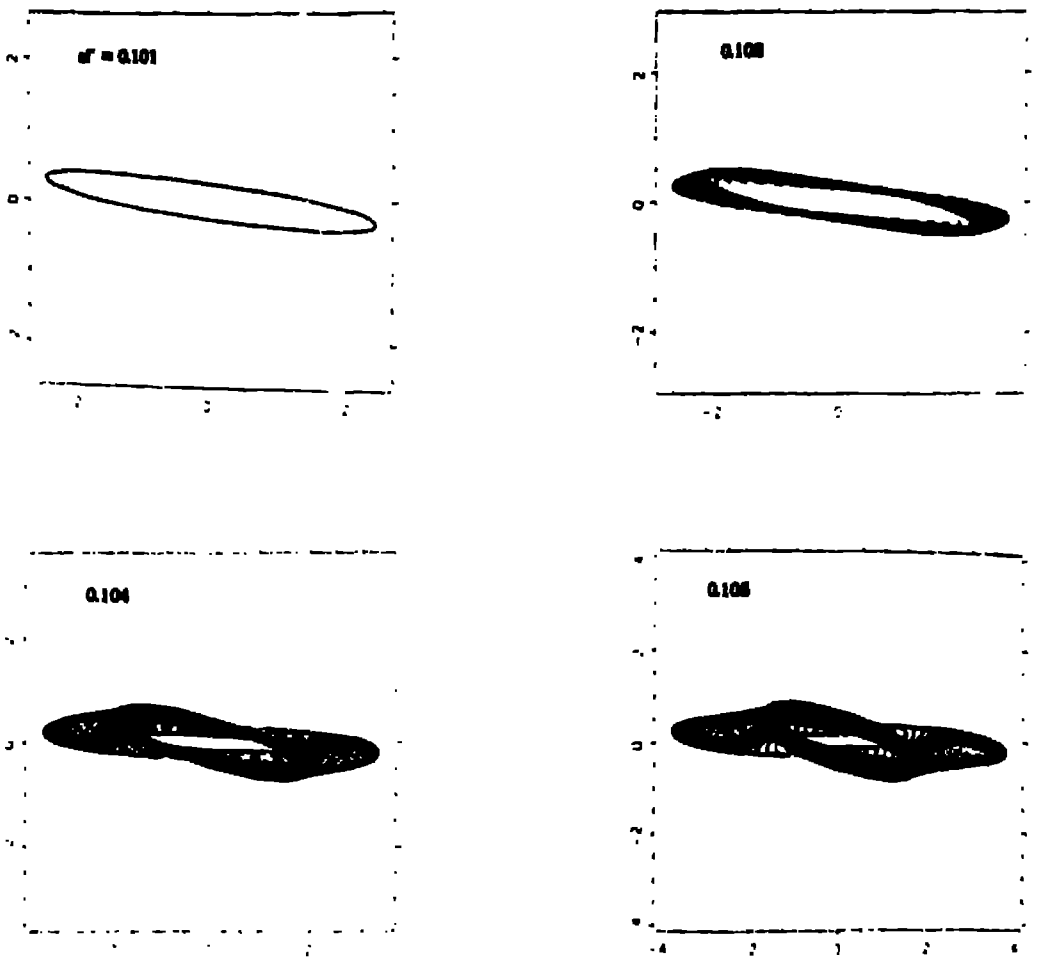

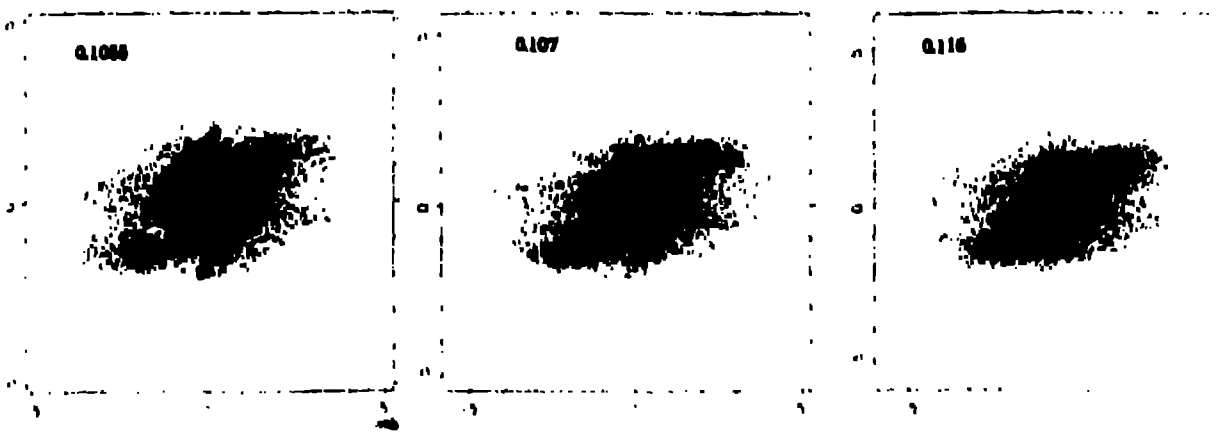

FIG. 5

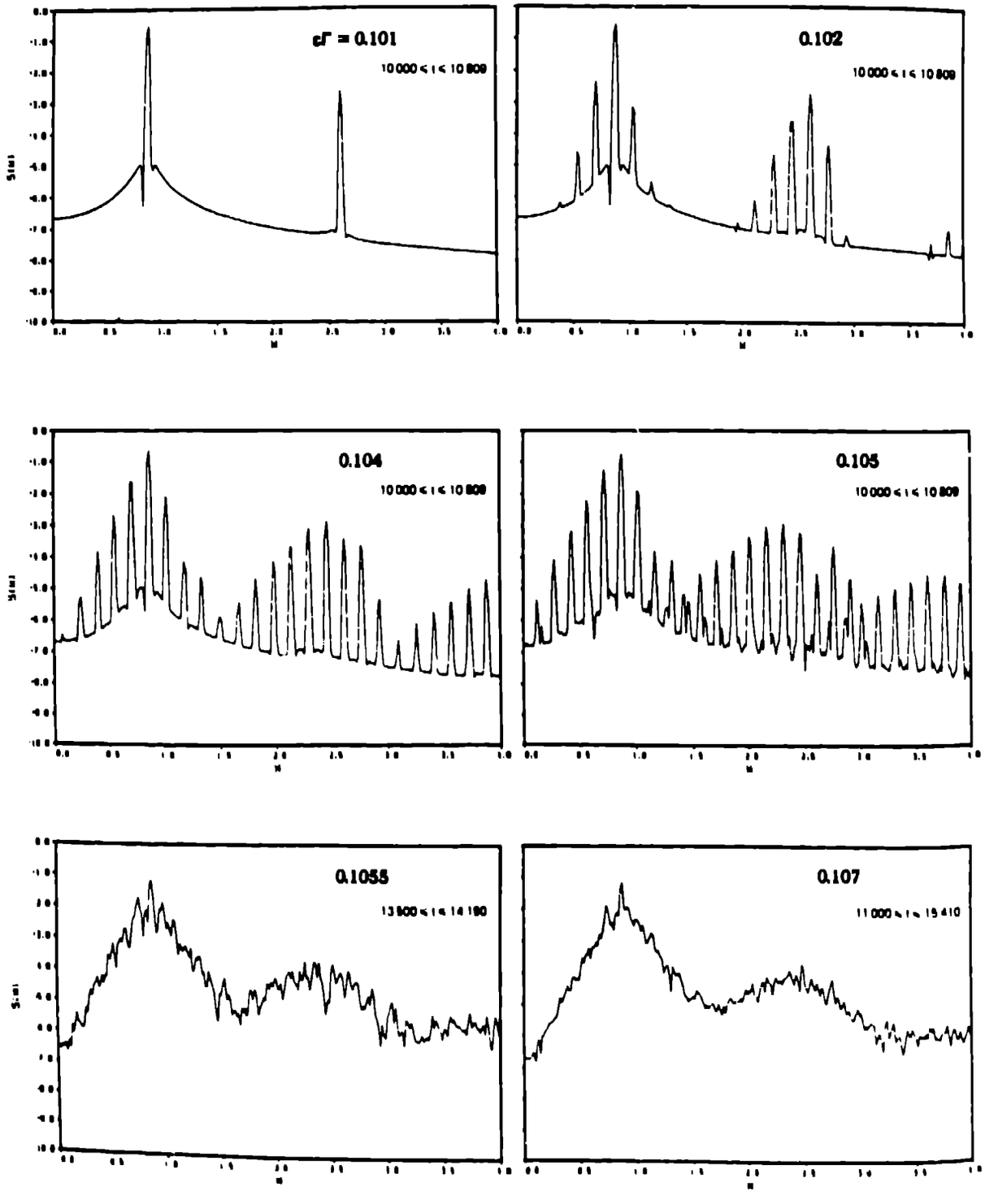
cΓ = 0.101
10000 < t < 10809
0.102
10000 < t < 10809
0.104
10000 < t < 10809
0.105
10000 < t < 10809
0.1055
13800 < t < 14190
0.107
11000 < t < 15410

Fig. (3a)

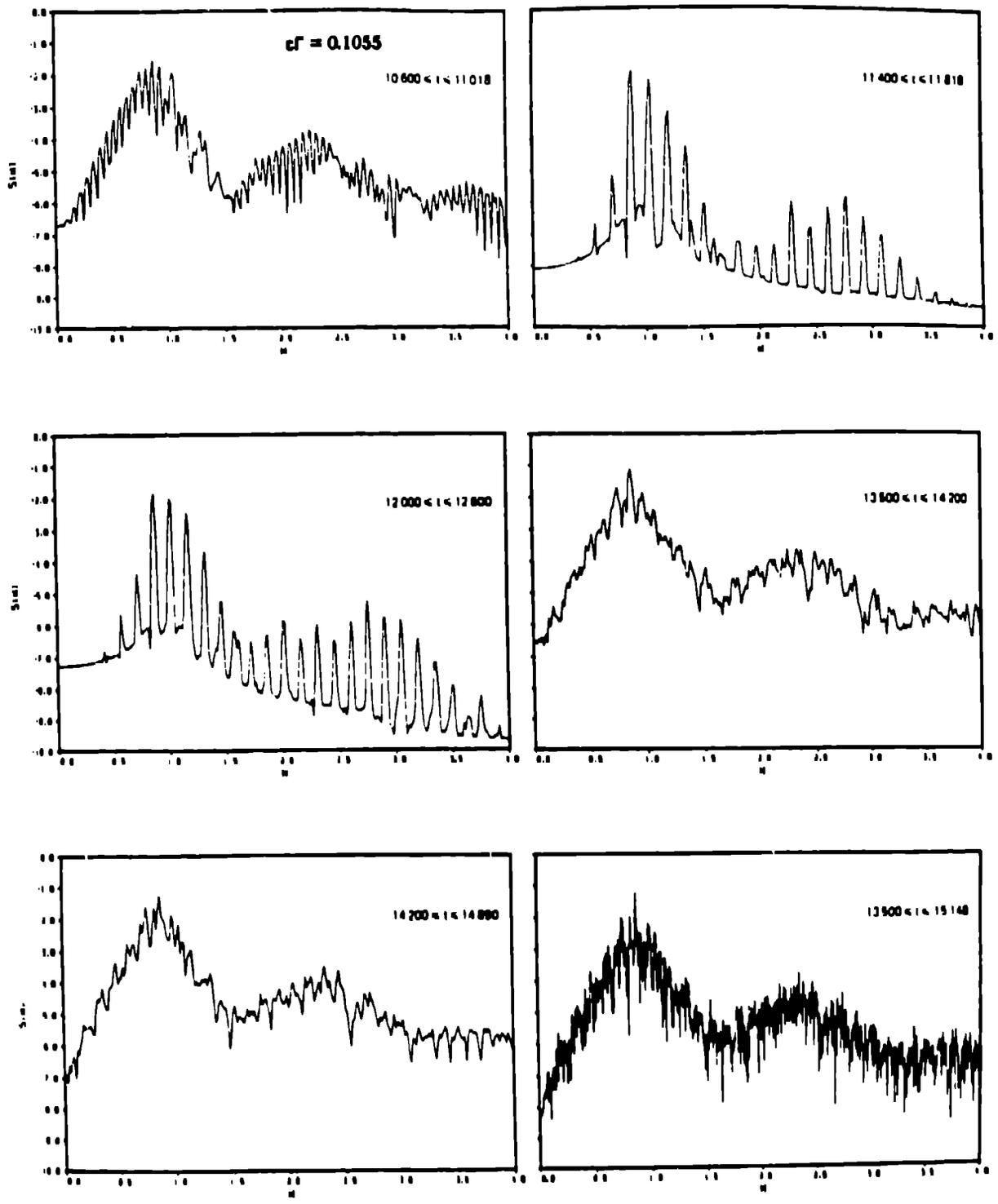
cr = 0.1055
10600 < t < 11018
11400 < t < 11818
12000 < t < 12800
13600 < t < 14200
14200 < t < 14890
13500 < t < 15148

Fig. 6b

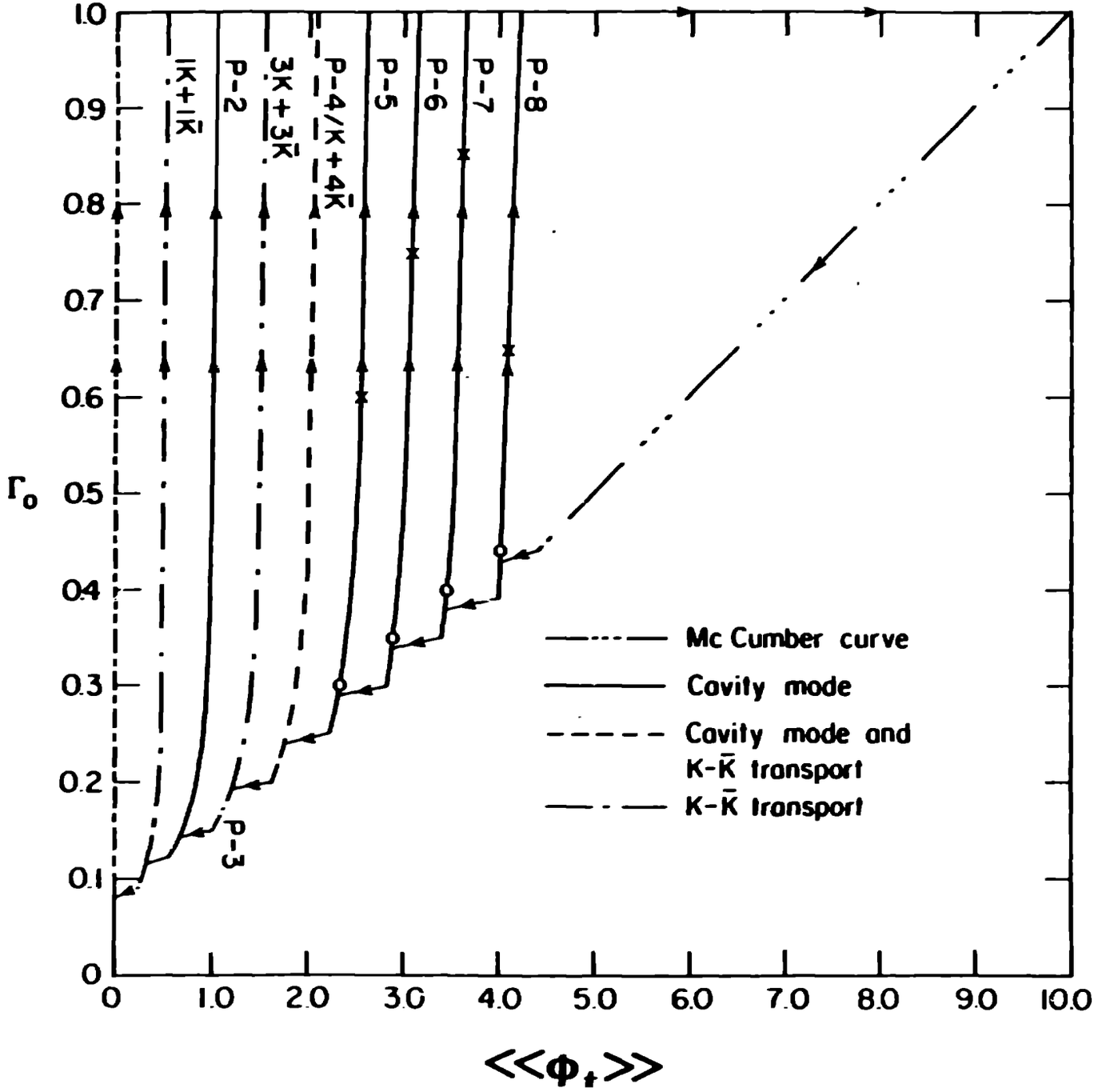
1.0
0.9
0.8
0.7
0.6
0.5
0.4
0.3
0.2
0.1
0
Γ_o
0
1.0
2.0
3.0
4.0
5.0
6.0
7.0
8.0
9.0
10.0
$\langle\langle\Phi_t\rangle\rangle$
1K+1$\bar{K}$
P-2
3K+3$\bar{K}$
P-4/K+4$\bar{K}$
P-5
P-6
P-7
P-8
P-3
Mc Cumber curve
Cavity mode
Cavity mode and K-$\bar{K}$ transport
K-$\bar{K}$ transport

FIG. 7.

(a)

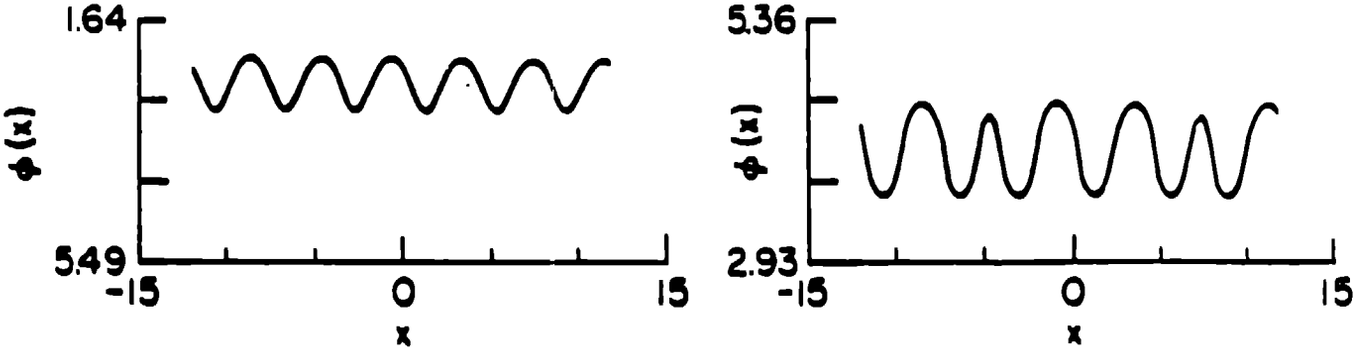
1.64
5.49
φ(x)
-15
0
15
x
5.36
2.93
φ(x)
-15
0
15
x

(b)

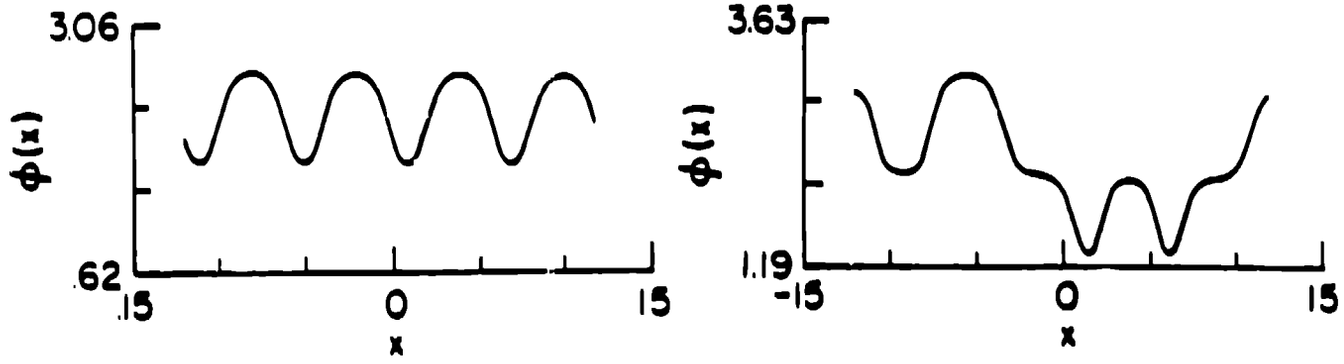
3.06
.62
φ(x)
.15
0
15
x
3.63
1.19
φ(x)
-15
0
15
x

FIG. 2

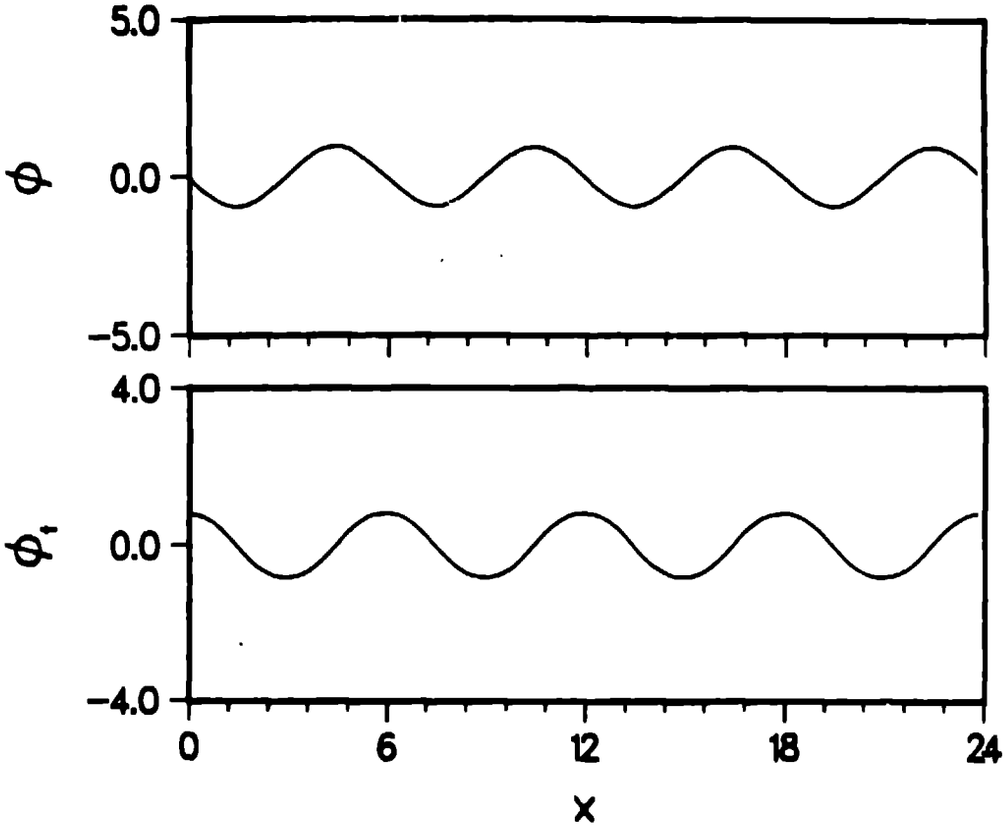

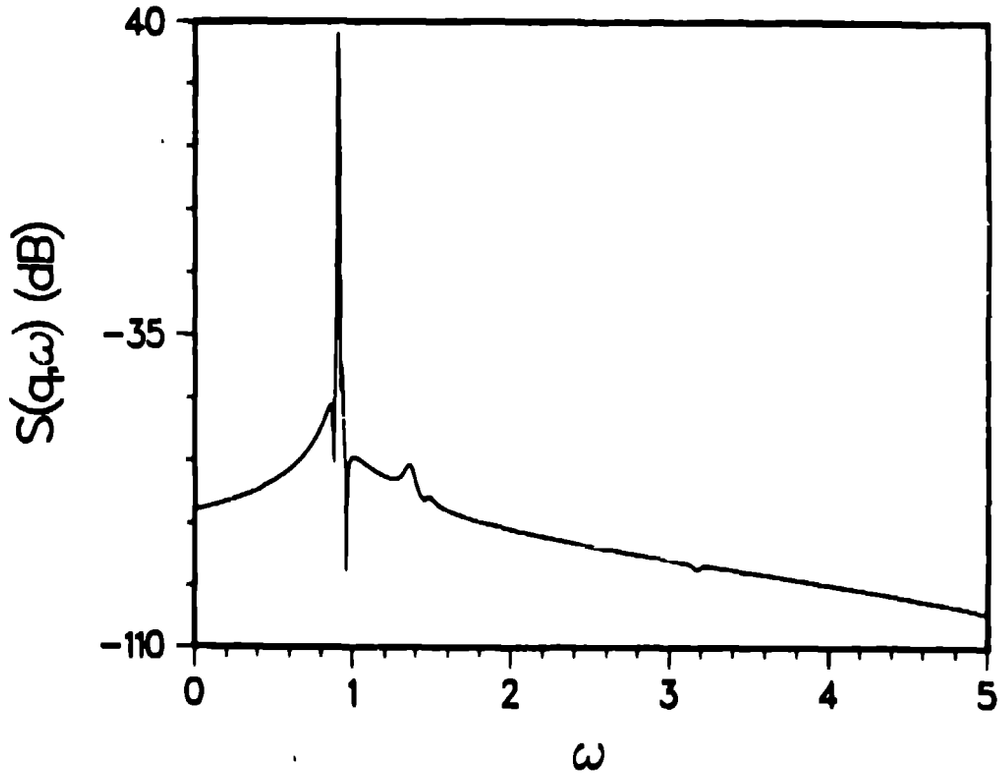

Fig. 9(a)

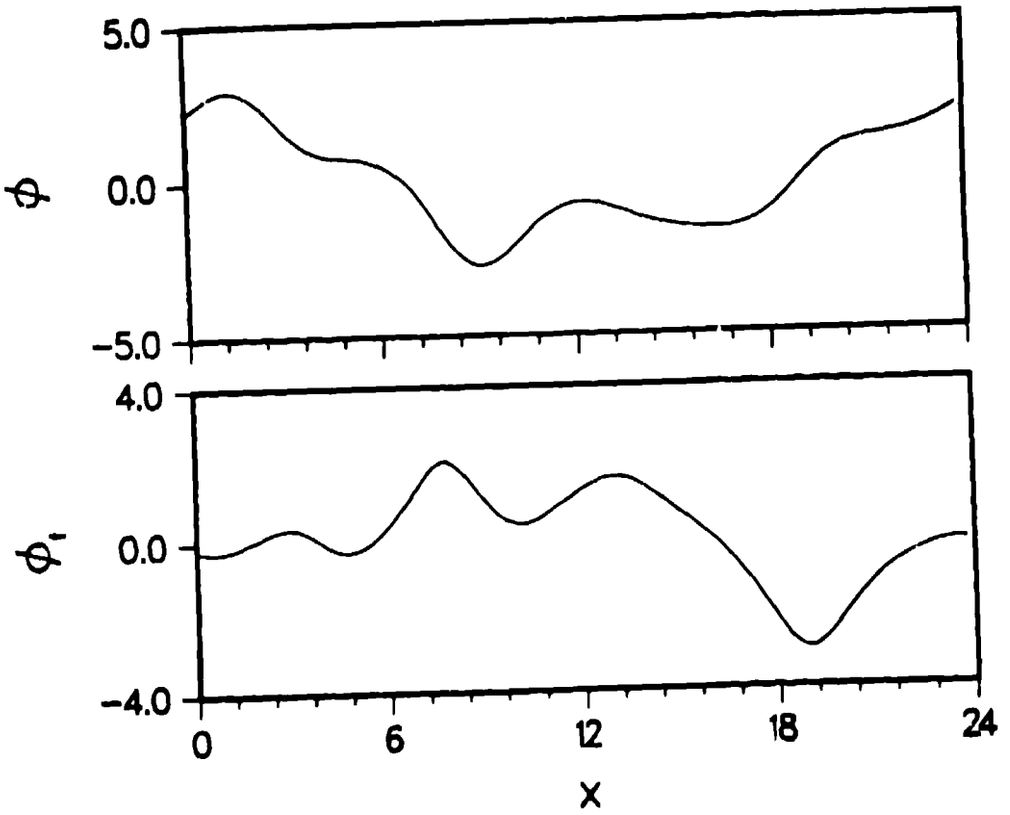

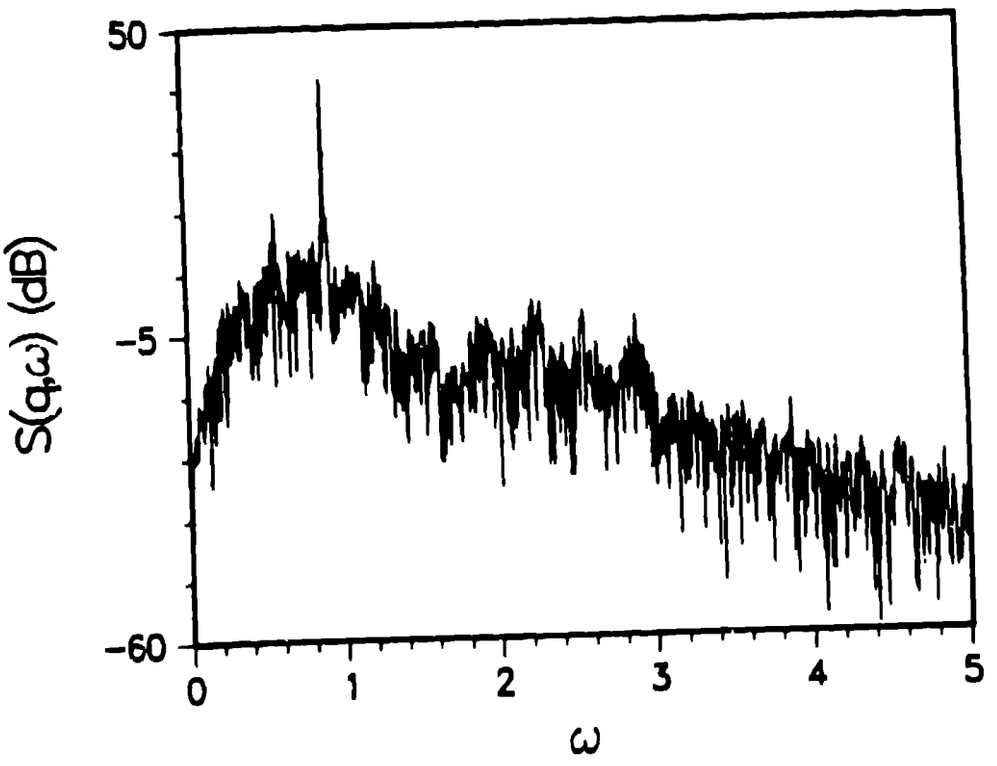

FIG. 1 (b)